REPORT

LIQUID DROPLET IN CONTACT WITH A SOLID SURFACE

S. Maruyama, T. Kurashige, S. Matsumoto, Y. Yamaguchi, and T. Kimura

Department of Mechanical Engineering, The University of Tokyo, Tokyo, Japan

A liquid droplet in contact with a solid surface was simulated by the molecular dynamics method, in order to study the microscopic aspects of the liquid–solid contact phenomena and phase-change heat transfer. Measured "contact angle" was well correlated by the depth of the integrated potential of the surface. The layered liquid structure near the surface was also explained with the integrated potential field. Furthermore, evaporation and condensation through the droplet were simulated by preparing two solid surfaces with temperature differences on the top and bottom of the calculation domain. Overall heat flux and temperature distributions of droplets were measured.

The microscopic mechanism of solid–liquid contact is fundamental to understanding phase-change phenomena such as dropwise condensation and the collapse of a liquid film on a heated surface. We have applied the molecular dynamics method to understand interphase phenomena such as surface tension [1, 2] and liquid–solid contact [3]. Our previous study [3] demonstrated that the droplet could be regarded as a semispherical shape except for a few layers of liquid structure on the surface, and that the cosine of the "contact angle" was a linear function of the energy scale of the interaction potential. In this report, by changing more parameters such as the length scale of the interaction potential, system size, and temperature, we give a more general description of the phenomenon. As surface molecules were expressed by a single layer of fixed molecules in the previous report, in this report we show two different levels of approximation for the surface: an even simpler one-dimensional function, and more complex three layers of harmonic molecules. Finally, through the simulation of actual phase change, the microscopic characteristics of heat transfer are discussed.

Received 12 August 1997; accepted 1 October 1997.

S. Matsumoto's present address is Mechanical Engineering Laboratory, Agency of Industrial Science and Technology/MITI, Ibaraki, Japan.

Address correspondence to Prof. Shigeo Maruyama, Department of Mechanical Engineering, The University of Tokyo, 7-3-1 Hongo, Bunkyo-ku, Tokyo 113, Japan. E-mail: maruyama@photon.t.u-tokyo.ac.jp

Microscale Thermophysical Engineering, 2:49–62, 1998

1089-3954/98 $12.00 + .00

EQUILIBRIUM DROPLET

Similar simulations as in the previous report [3] were performed with the modification of the surface condition. A molecular dynamics simulation was designed to achieve an equilibrium state of the liquid droplet and its vapor on a solid surface under the *NVE* ensemble. Figure 1 illustrates the initial configuration and liquid–vapor equilibrium condition after 1,000 ps. Here, the liquid and vapor molecules were distinguished by the potential field felt by each molecule. The liquid droplet and the vapor consisted of Lennard-Jones molecules with the interaction potential expressed as

$$\phi(r) = 4\varepsilon\left[\left(\frac{\sigma}{r}\right)^{12} - \left(\frac{\sigma}{r}\right)^{6}\right] \tag{1}$$

For physical insights, we regarded the molecule as argon with the potential parameters set as: $\sigma_{\mathrm{AR}} = 3.4$ Å, $\varepsilon_{\mathrm{AR}} = 1.67 \times 10^{-21}$ J. The calculation region had periodic boundaries for four side surfaces and a mirror boundary (or a hard wall boundary) for the top surface. The bottom surface was expressed by either a one-dimensional potential function, a fixed single layer of solid molecules, or three layers of harmonic molecules. We modeled the fcc (1, 1, 1) surface with the nearest-neighbor distance $\sigma_S = 2.77$ Å, the spring constant $k = 46.8$ N/m, and mass $m_S = 32.39 \times 10^{-26}$ kg (the platinum crystal was modeled). The interaction potential between solid and argon molecules was also expressed by the Lennard-Jones potential with the parameters σ_{INT} and $\varepsilon_{\mathrm{INT}}$. For the one-dimensional

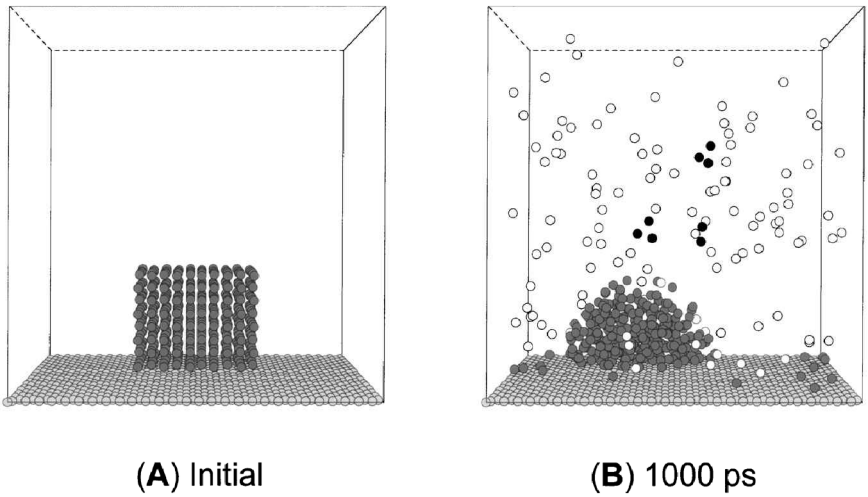

Figure 1. Snapshots of a liquid droplet on the solid surface. Gray, dark gray, and white circles correspond to solid, liquid, and vapor molecules, respectively.

potential function we have integrated one layer of the fcc (1, 1, 1) surface as

$$\Phi(z) = \frac{4\sqrt{3}\,\pi}{15}\,\frac{\varepsilon_{\mathrm{INT}}\,\sigma_{\mathrm{INT}}^2}{\sigma_S^2}\left\{2\left(\frac{\sigma_{\mathrm{INT}}}{z}\right)^{10} - 5\left(\frac{\sigma_{\mathrm{INT}}}{z}\right)^{4}\right\} \tag{2}$$

where z is the coordinate normal to the surface. Another one-dimensional function is available in a textbook [4]: the full integration of uniform solid molecules. However, we believe that our form of one-layer integration must give a better representation of the potential field very near the surface, and that it is suitable for a direct comparison with our other representations of the surface. The second and third solid layers can be taken into account by adding the same function with a shift of z of the lattice constant. Here, it should be noticed that the minimum $\varepsilon_{\mathrm{SURF}}$ of this function in Eq. (2) appears when $z = \sigma_{\mathrm{INT}}$ as

$$\varepsilon_{\mathrm{SURF}} = \left(\frac{4\sqrt{3}\,\pi}{5}\right)\left(\frac{\sigma_{\mathrm{INT}}^2}{\sigma_S^2}\right)\varepsilon_{\mathrm{INT}} \tag{3}$$

The equation of motion was integrated numerically utilizing the Verlet algorithm [4] with a time step of 0.01 ps. Equilibration and data acquisition were the same as in our previous report [3]. Note that the effect of the initial condition was negligible for the equilibrium results, and the same equilibrium state could be obtained even from a dense gas-phase initial condition.

Figure 2 shows the two-dimensional density profiles [3] for various sizes of droplets. With the increase of the number of liquid molecules, the relative percentage of bulk liquid increases. The contact angle θ was measured by fitting a circle to the density contour, ignoring the layered part as before [3]. It is rather surprising that the contact angle was nearly the same even with only a few hundred molecules constituting the droplet. The smaller droplet was made mostly of the layered structure [5], and the measurement of the contact angle was difficult.

The effect of the temperature on the contact angle was too small to be described within our uncertainty, though the two-dimensional density distributions seemed quite different. The liquid–vapor interface was more diffuse, and the first liquid layer was more prominent for higher temperature.

It was found that the contact angle was correlated with the integrated depth of the surface potential $\varepsilon_{\mathrm{SURF}}$ [see Eq. (3)], as demonstrated in Figure 3. Parameters of the interaction potential σ_{INT} and $\varepsilon_{\mathrm{INT}}$ were changed from complete wetting ($\theta = 0^\circ$) through complete drying ($\theta = 180^\circ$), as shown in Table 1. The representation of the surface molecules did not affect the result as long as the $\varepsilon_{\mathrm{SURF}}$ was the same. Furthermore, the two-dimensional density and potential distributions were almost nondistinguishable among three different surface conditions.

Here, the well-known Young's equation for the macroscopic contact angle is expressed as

$$\cos\theta = (\gamma_{sg} - \gamma_{sl})/\gamma_{lg} \tag{4}$$

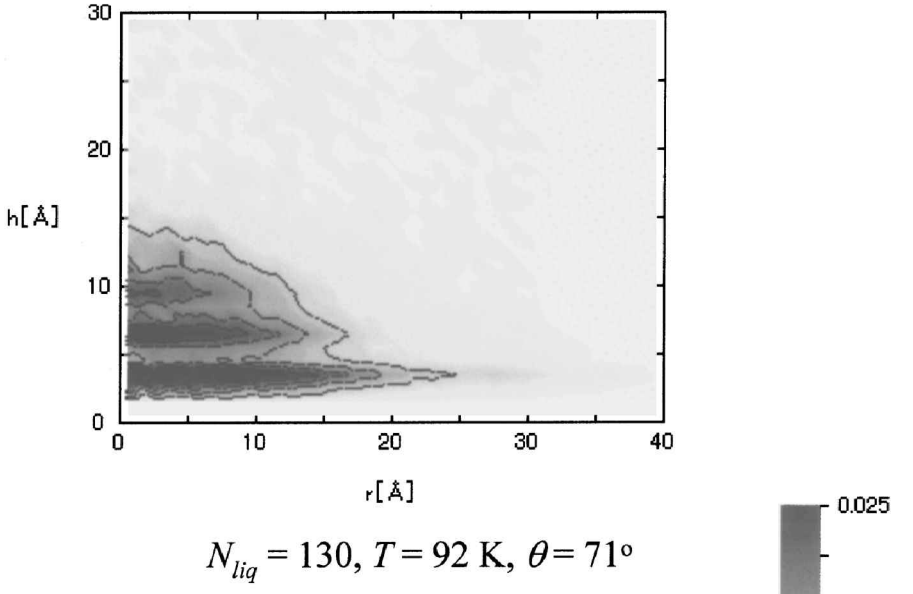

(*a*)

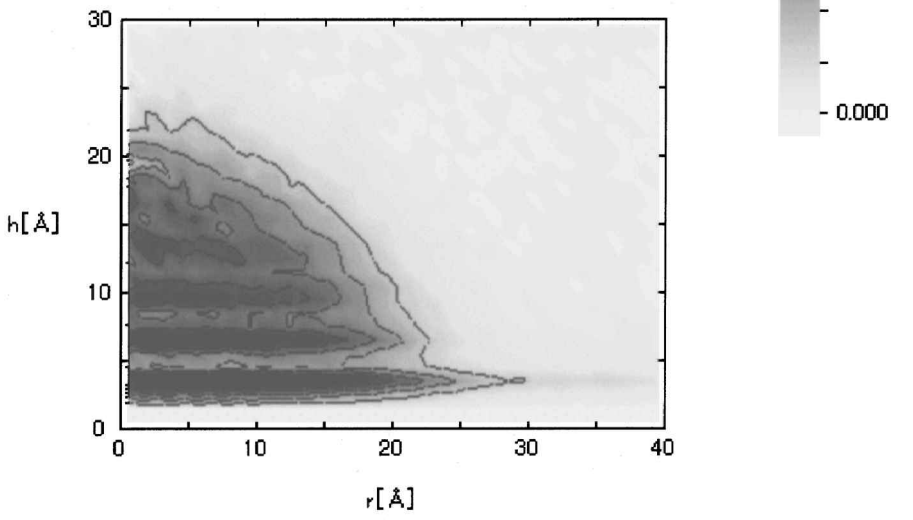

(*b*)

Figure 2. The effect of liquid size on the two-dimensional density profile.

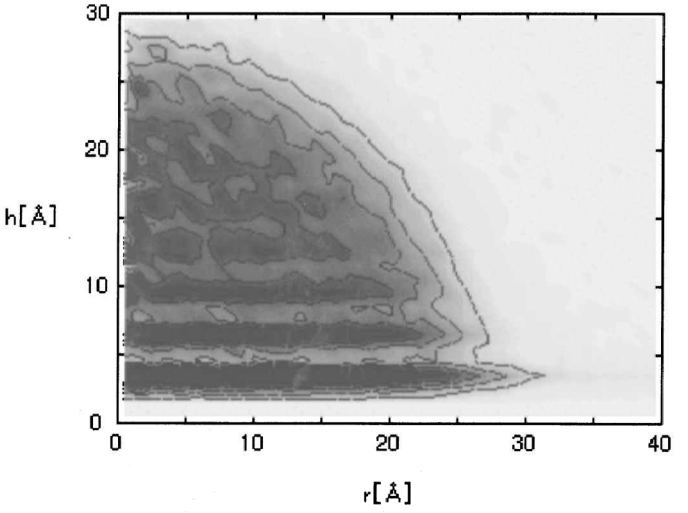

$N_{liq} = 700,\ T = 92\ \text{K},\ \theta = 94^{\circ}$

(*c*)

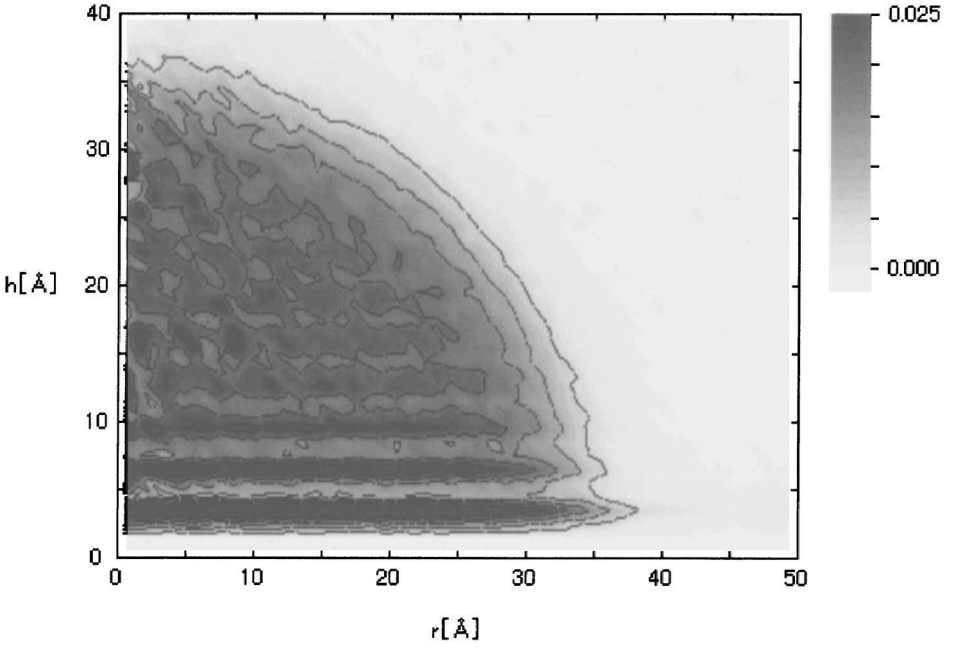

$N_{liq} = 1600,\ T = 92\ \text{K},\ \theta = 90^{\circ}$

(*d*)

Figure 2. The effect of liquid size on the two-dimensional density profile (*Continued*).

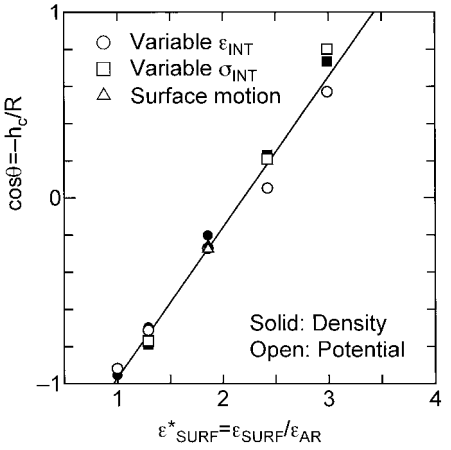

Figure 3. Dependence of the contact angle on the depth of the integrated potential. Variable ε_{INT} and σ_{INT} correspond to conditions E x and S x in Table 1, respectively.

where γ_{sg}, γ_{sl}, and γ_{lg} are the surface energies of the solid–vapor, solid–liquid, and liquid–vapor interfaces, respectively. Even though the early molecular dynamics study concluded that the Young's equation was not applicable to the microscopic system [6], later studies suggested opposite results [7, 8]. If we assume that the difference of the solid-related surface energy $\gamma_{sg} - \gamma_{sl}$ is proportional to the potential parameter as expected from [7, 8], our result supports Young's equation for the main body of the droplet.

The layered structure is unique to the microscopic droplets. As the droplet size becomes smaller, characteristics of this structure dominate the whole shape as shown in Figure 2. Figure 4 compares the profiles of liquid density for various energy scales ε_{INT}. The first peak appeared at σ_{INT} from the solid molecule, and successive peaks appeared at intervals of σ_{AR} (a similar picture with varying σ_{INT} supported this relationship). These relations can be clearly understood by considering Figure 5, which compares the density profile with the integrated potential function. The similarity of the density profile and the integrated potential suggests that the density profile is simply determined by the effective potential field and the temperature. As the first liquid layer is built up by the surface molecules, it works as the imperfect surface for the second liquid layer and so on.

INEQUILIBRIUM DROPLET (PHASE-CHANGE HEAT TRANSFER)

Characteristics of phase-change heat transfer were studied with the system as shown in Figure 6. Solid surfaces on the top and bottom of the calculation domain were represented by three layers of harmonic molecules with additional "phantom" molecules [9]. The phantom molecules, which mimicked the continuous bulk solid, were introduced to give constant-temperature boundary conditions. Solid molecules in the third layer were connected to phantom molecules through springs (the vertical and horizontal spring constants were $0.5k$ and $2k$, respectively). Then, phantom molecules were connected to the fixed frame by springs (the vertical and horizontal constants were $3.5k$ and $2k$, respectively) and dampers with the damping

Table 1. Calculation conditions and contact angle

				One-dimensional function					Fixed one-layer				
Label	ε_{INT} [$\times 10^{-21}$ J]	σ_{INT} [Å]	ε^*_{SURF}	T [K]	N_v	R [Å]	θ_{DNS} [deg]	θ_{POT} [deg]	T [K]	N_v	R [Å]	θ_{DNS} [deg]	θ_{POT} [deg]
E0	0.309	3.085	1.00	89.5	113	14.9	149.6	153.5	90.0	125	14.7	157.0	162.9
E1	0.400	3.085	1.29	91.9	110	15.2	139.1	142.6	95.1	134	15.0	135.4	134.1
E2	0.575	3.085	1.86	90.8	101	17.4	105.2	104.5	94.6	113	17.0	105.8	101.7
E3	0.750	3.085	2.42	94.8	105	20.2	85.5	87.9	94.4	101	19.6	87.0	87.0
E4	0.925	3.085	2.99	94.2	93	33.0	51.0	52.2	93.9	87	30.6	55.2	55.6
E5	1.100	3.085	3.56	94.5	76	$\sim \infty$	0	0					
S1	0.575	2.573	1.29	92.7	115	14.8	149.2	157.3	94.2	125	14.8	140.4	142.3
S3	0.575	3.523	2.42	91.4	96	20.3	84.2	81.6	93.7	114	21.4	77.9	76.6
S4	0.575	3.913	2.99	90.7	75	53.6	36.8	44.9	95.5	86	54.2	36.8	42.9
									3-layers of harmonic molecules				
V2	0.468	3.085	1.86						92.2	128	16.7	106.0	140.6

$\varepsilon^*_{SURF} = \varepsilon_{SURF}/\varepsilon_{AR}$; T, temperature; N_v, number of vapor; R, radius of fitting circle, θ_{DNS}, contact angle measured from density profile; θ_{POT}, contact angle measured from potential profile.

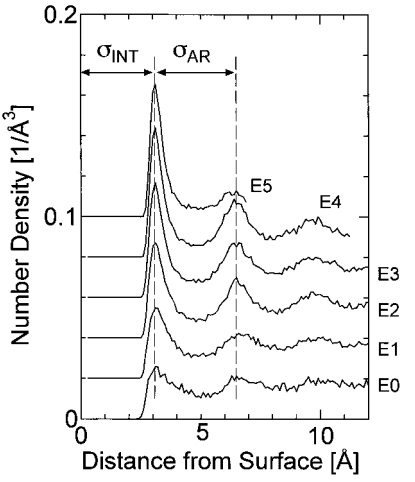

Figure 4. Density distributions of liquid near the solid surface. See Table 1 for E x labels.

constant $\alpha = 5.184 \times 10^{-12}$ [kg/s]. The phantom molecules were further excited by artificial random force with standard deviation $\sigma_F = \sqrt{2\alpha k_B T/\Delta t}$, where k_B is the Boltzmann constant and Δt is the time step.

Figure 7 shows the time sequence of the calculation. We prepared a solid surface and a droplet separately in equilibrium at 100 K, and merged them to the configuration of Figure 6. Then, after calculating 200 ps for the relaxation, top and bottom phantom molecules were suddenly set to 85 and 115 K, respectively. The phase-change process can be clearly seen in the change of the number of molecules N_L^{cond} (droplet in condensing side), N_L^{evap} (evaporating side), and N_V (vapor) in the bottom panel of Figure 7. Since N_V was almost constant, the condensation rate and the evaporation rate were almost the same. The temperature of the solid surfaces T_S^{evap} (bottom) and T_S^{cond} (top) quickly jumped to the phantom temperature, but the temperature difference of the two liquid droplets was very small. This

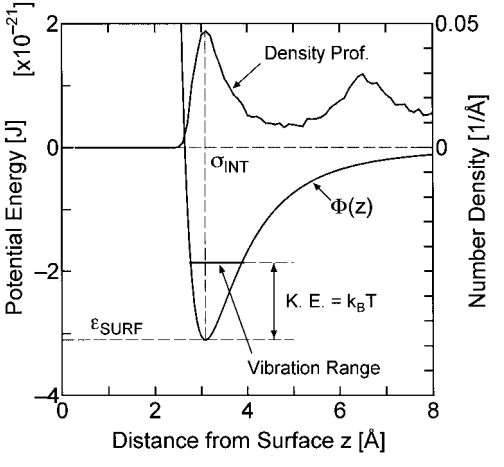

Figure 5. Relationship of the density profile and the integrated potential function (E2 condition in Table 1).

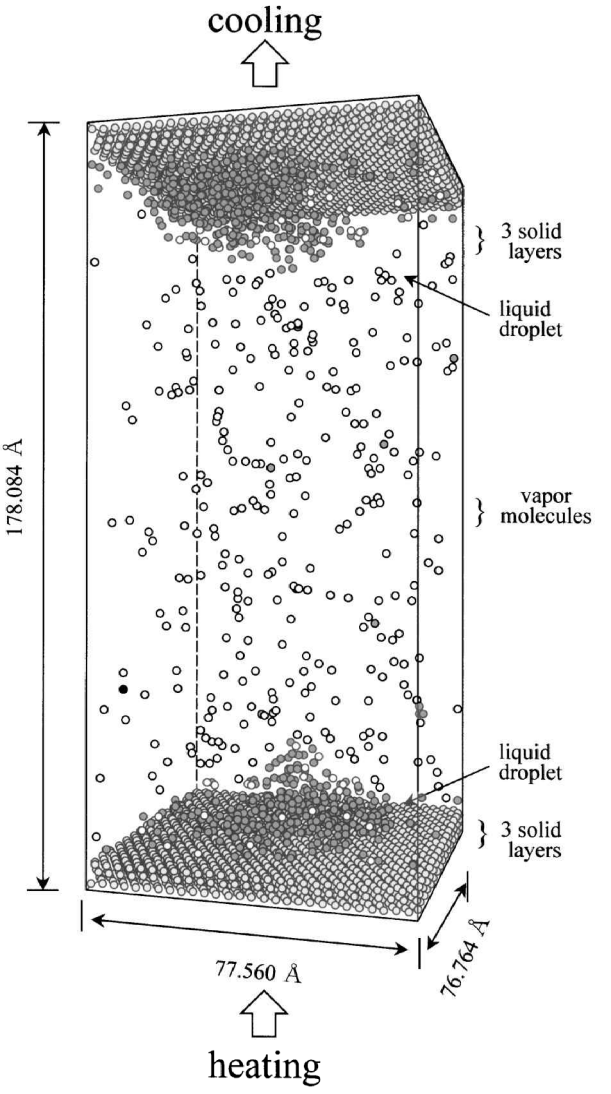

Figure 6. A snapshot of inequilibrium droplets on solid surfaces.

result showed that the liquid–solid contact thermal resistance was dominant compared with heat conduction and phase-change thermal resistances. We assumed that the heat transfer was quasi-steady (the rate of phase change was constant) after 500 ps, and measured the heat flux, velocity, and temperature distributions. The average heat flux measured at the middle of the calculation domain was 24 MW/m^2, which is the order of the maximum heat flux possible in phase change.

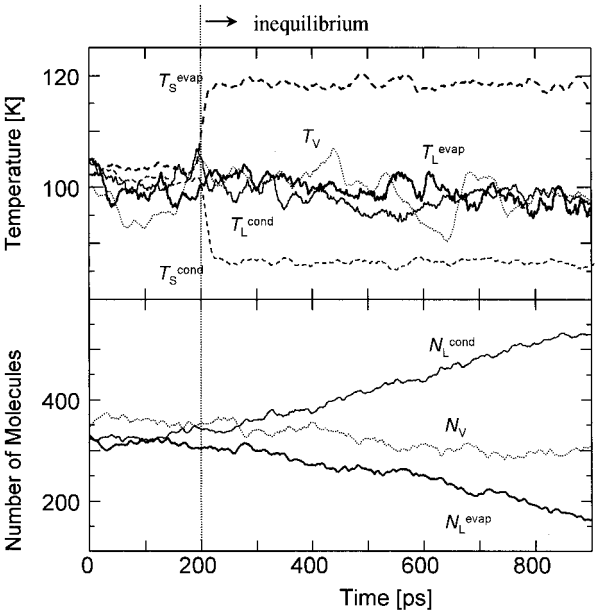

Figure 7. Variations of temperature and number of molecules. T and N are temperature and number of molecules, respectively. Subscripts S, L, and V represent solid, liquid, and vapor, respectively, and superscripts evap and cond represent evaporation side (bottom) and condensation side (top), respectively.

Figure 8 shows the velocity and temperature distributions on the evaporation side. The velocity distribution compared with the density distribution (top panel of Figure 8) shows that the evaporation at the three-phase contact line (or the first layer of liquid) was most dominant, and some supply flow of liquid from the middle of the droplet to the first layer was observed. The higher droplet temperature at the three-phase contact line also supports this observation. The temperature of the first layer of the solid was lower under this area and higher under the center of the droplet due to the thermal insulation provided by the liquid.

The same representations on the condensing side are shown in Figure 9. Here, the specialness at the three-phase contact line was less pronounced, and rather uniform condensation was observed over the whole liquid surface. The temperature distribution of the liquid exhibited a simple linear increase along the z direction, and the decrease of solid surface temperature at the center is simply explained by the thermal insulating effect of the liquid droplet.

The measured contact angle was almost the same for both condensing and evaporating droplets, as recognized in Figures 8 and 9. It seems that the contact angle was principally determined by the surface energy balance and was not very sensitive to the lower-energy temperature distributions.

We noticed that three-layer solid molecules had been too thin to consider such a problem with the temperature distribution in the radial direction. Even though we were confident of the use of the phantom technique through equilib-

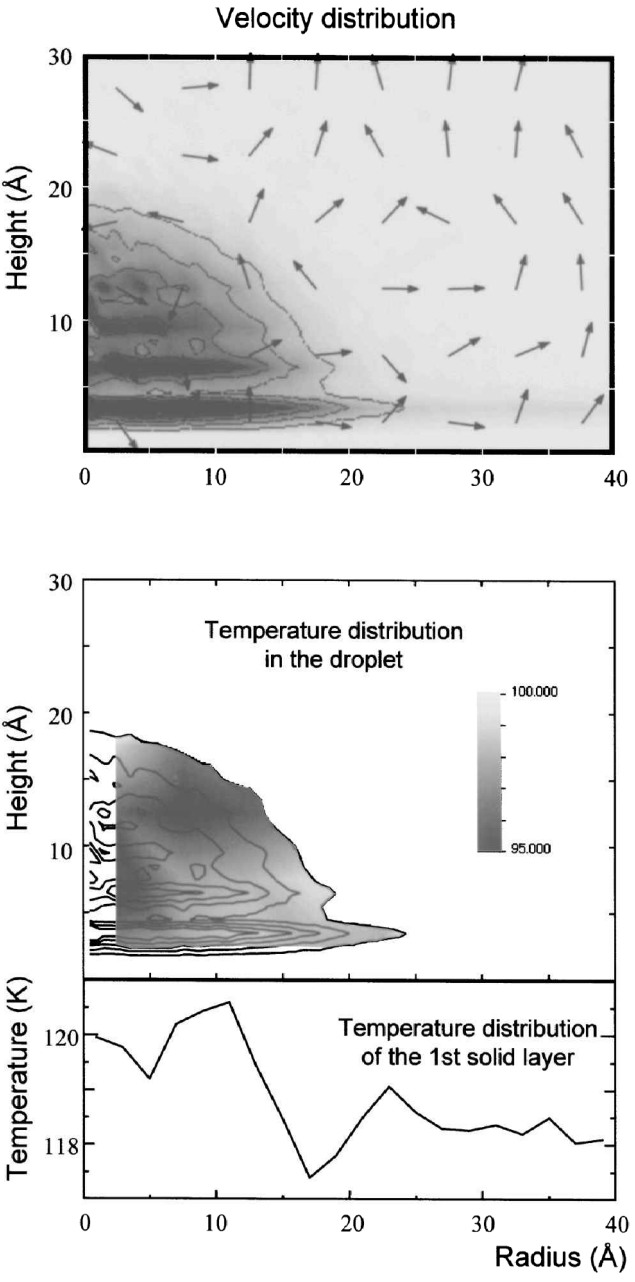

Figure 8. Characteristics of evaporating droplet. *Top*, density profile and velocity vectors; *middle*, temperature distribution in the droplet; *bottom*, temperature distribution of the first layer of solid surface.

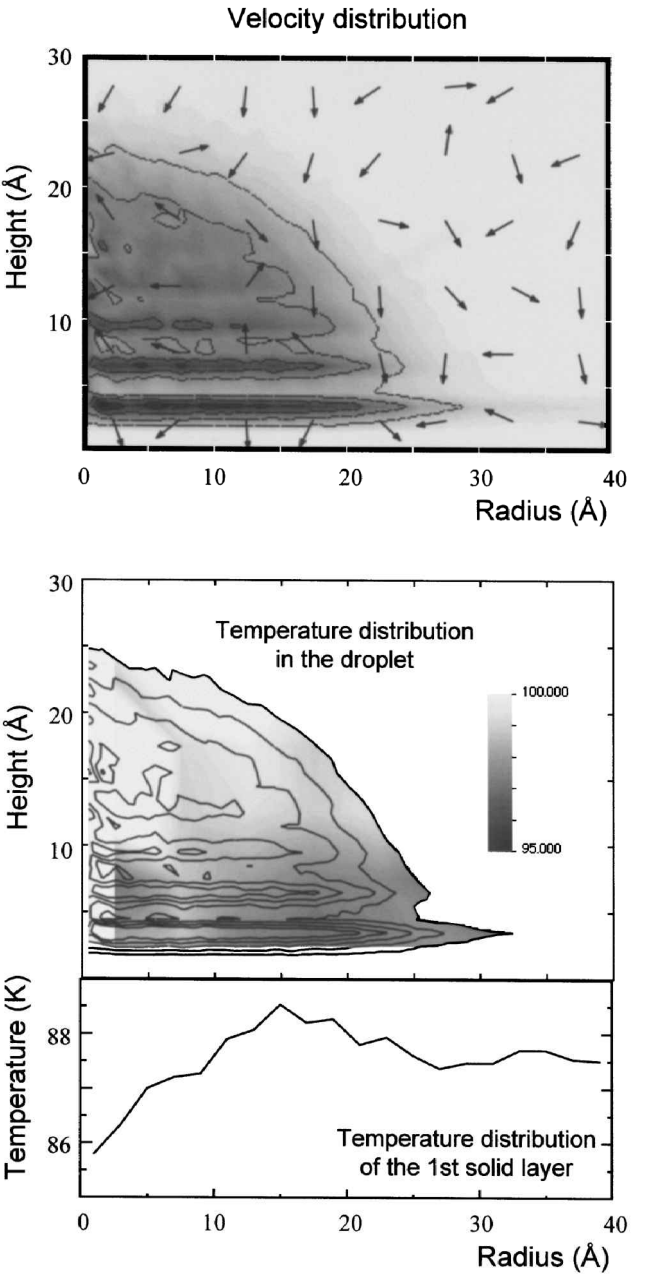

Figure 9. Characteristics of condensing droplet. *Top*, density profile and velocity vectors; *middle*, temperature distribution in the droplet; *bottom*, temperature distribution of the first layer of solid surface.

rium calculations of other systems, imposing the uniform temperature just three layers below the first layer with temperature distribution as seen in Figures 8 and 9 was actually unacceptable. If we could use reasonably thicker solid layers, probably the solid-layer temperature distribution would be more pronounced. Furthermore, the slight upper shift (about 3 K) of the solid temperature from the phantom set value observed in Figure 7 seems to be due to this problem. Even though computer time and memory crucially limit the number of solid molecules, calculations with a thicker solid layer are desired in the future.

CONCLUSIONS

A liquid droplet in contact with a solid surface was simulated by the molecular dynamics method. The liquid droplet and surrounding vapor were realized by Lennard-Jones molecules, and the solid surface was represented by three types of models: three layers of harmonic molecules, one layer of fixed molecules, or a simple one-dimensional function. The interaction potential between solid molecules and liquid/vapor molecules was represented by the Lennard-Jones potential with various length and energy parameters.

It was found that the cosine of the contact angle was well expressed by a linear function of the depth of the integrated interaction potential, regardless of surface representations. Assuming that the surface energy was proportional to the potential depth, the macroscopic Young's equation was still valid even for such a small droplet. On the other hand, the layered structure that appeared in the two-dimensional density profile of droplet was well explained through the shape of the integrated interaction potential.

By preparing two solid surfaces with different temperatures, evaporation in one droplet and condensation on the other were simulated simultaneously. The contact angle was almost the same as the equilibrium condition. Velocity and temperature distributions of droplets evaporating and condensing as well as the heat flux were measured for the quasi-steady condition. The importance of the three-phase contact line in the evaporation process, in clear contrast to the condensation process, was observed.

REFERENCES

1. S. Maruyama, S. Matsumoto, and A. Ogita, Surface Phenomena of Molecular Clusters by Molecular Dynamics Method, *Thermal Sci. Eng.*, vol. 2, no. 1, pp. 77–84, 1994.
2. S. Maruyama, S. Matsumoto, M. Shoji, and A. Ogita, A Molecular Dynamics Study of Interface Phenomena of a Liquid Droplet, *Proc. 10th Int. Heat Transfer Conf.*, vol. 3, pp. 409–414, Brighton, U.K., 1994.
3. S. Matsumoto, S. Maruyama, and H. Saruwatari, A Molecular Dynamics Simulation of a Liquid Droplet on a Solid Surface, *Proc. ASME/JSME Thermal Engineering Joint Conf.*, vol. 2, pp. 557–562, Maui, HI, 1995.
4. M. P. Allen and D. J. Tildesley, *Computer Simulation of Liquids*, Oxford University Press, Oxford, 1987.
5. J. N. Israelachvili, *Intermolecular and Surface Forces*, Academic Press, London, 1985.
6. G. Saville, Computer Simulation of the Liquid-Solid-Vapour Contact Angle, *J. Chem. Soc. Faraday Trans. 2*, vol. 73, pp. 1122–1132, 1977.

7. J. H. Sikkenk, J. O. Indekeu, J. M. J. van Leeuwen, E. O. Vossnack, and A. F. Bakker, Simulation of Wetting and Drying at Solid-Fluid Interfaces on the Delft Molecular Dynamics Processor, *J. Stat. Phys.*, vol. 52, no. 1/2, pp. 23–44, 1988.
8. M. J. P. Nijmeijer, C. Bruin, and A. F. Bakker, Wetting and Drying of an Inert Wall by a Fluid in a Molecular-Dynamics Simulation, *Phys. Rev. A*, vol. 42, no. 10, pp. 6052–6059, 1990.
9. J. Blömer and A. E. Beylich, MD-Simulation of Inelastic Molecular Collisions with Condensed Matter Surfaces, Proc. 20th Int. Symp. on Rarefied Gas Dynamics, pp. 392–397, Beijing, China, 1997.